Journal of Luminescence 195 (2018) 216–224

Contents lists available at ScienceDirect

Journal of Luminescence

journal homepage: www.elsevier.com/locate/jlumin

Anomalous fading in TL, OSL and TA – OSL signals of Durango apatite for various grain size fractions; from micro to nano scale

G.S. Polymeris[a,*], I.K. Sfampa[b], M. Niora[b], E.C. Stefanaki[c], L. Malletzidou[c], V. Giannoulatou[a], V. Pagonis[d], G. Kitis[b]

[a] Institute of Nuclear Sciences, Ankara University, Beşevler, 06100 Ankara, Turkey
[b] Nuclear Physics Laboratory, Physics Department, Aristotle University of Thessaloniki, 54124 Thessaloniki, Greece
[c] Solid State Physics section, Physics Department, Aristotle University of Thessaloniki, 54124 Thessaloniki, Greece
[d] McDaniel College, Physics Department, Westminster, MD 21157, USA

ARTICLE INFO

Keywords:
Anomalous fading
TL/OSL
Tunneling recombination
Nano-scale
TA – OSL
Fluorapatite

ABSTRACT

Anomalous fading (AF) of luminescence signals has been studied extensively both experimentally and by simulations. This paper reports a new type of study of anomalous fading in grains of Durango apatite, a naturally occurring luminescent material that yields very intense anomalous fading. Grains of Durango apatite were ball milled (BM) for various durations, up to 48 h. Different ball milling durations resulted in different average grain size fractions as low as 200 nm, as it was indicated by Scanning Electron Microscopy (SEM) measurements. The anomalous fading effect was studied for optically stimulated luminescence (OSL), thermoluminescence (TL), as well as thermally-assisted OSL signals (TA – OSL). Anomalous fading was found to be ubiquitous for all luminescence signals, and for all apatite grain size fractions. The anomalous fading rate is weakly affected by the grain size for the cases of OSL and TL, while the TA – OSL signals were found to fade in a much slower rate than either the TL or the conventional OSL signals. An important experimental result is that the fading rate of TA – OSL decreases as the grain size fraction is decreased. For average grain size fractions between 200 and 450 nm, the TA – OSL signal is unaffected by the AF effect. A differential analysis on the TL glow curves showed that the AF rate decreases with increasing temperature along the glow curve, and also with increasing BM time. Finally, a component resolved de-convolution analysis was performed for both OSL and TA – OSL decay curves and recombination lifetimes are reported for both localized and delocalized components. FTIR analysis indicates that the ball milling procedure does not induce a new phase in this material.

1. Introduction

Anomalous fading (hereafter AF) of thermoluminescence (TL) signals is the term adopted for the rapid decay of luminescence at room temperature, instead of the stability expected for it according to standard luminescence kinetic models [1–7]. During the last 20 years, AF has also been studied in optically stimulated luminescence (OSL) and infrared stimulated luminescence (IRSL) signals [2,4–7]. It is now well established [8,9,12] that the AF effect is due to quantum mechanical tunneling, which is an important mechanism for loss of trapped electrons, inducing a source of signal instability in many types of phosphors. This loss of charge can take place directly from the ground state [11], or can be forced via an external stimulus through the excited state of the electron trap [13,14]. Recently Jain et al. [14] proposed a comprehensive model for the latter case, which will be referred to in this paper as localized tunneling recombination (LTR) model. In this model thermal or optical stimulation raises the trapped electrons into a higher energy level, from which they tunnel to the nearest neighbor luminescence center and recombine emitting light. Two important parameters of the LTR model are the trap-to-recombination center distance and a dimensionless parameter termed ρ′, which represents the concentration of the luminescence centers [14]. Kitis and Pagonis [15] quantified the semi-analytical model of Jain et al. [14] by deriving exact analytical expressions for different experimental stimulation modes. Later on, Pagonis et al. [16] obtained approximate expressions for the time development of nearest neighbor distribution during various types of luminescence experiments. Jain et al. [17] have extended their LTR model [14] by introducing Arrhenius analysis, and by analyzing IRSL signals that arise from truncated nearest-neighbor distributions.

Besides feldspar minerals which yield moderate AF, Durango apatite stands as an example of a material exhibiting very strong anomalous

* Corresponding author.
E-mail addresses: gspolymeris@ankara.edu.tr, polymers@auth.gr (G.S. Polymeris).

https://doi.org/10.1016/j.jlumin.2017.11.034
Received 7 March 2017; Received in revised form 16 November 2017; Accepted 20 November 2017
Available online 22 November 2017

fading; this mineral has been thoroughly studied as a reference material for AF studies [2,3,18–22]. It was shown that the AF phenomenon is ubiquitous in TL, OSL and IRSL signals of Durango apatite. In this material the AF of TL signals was studied as a function of (a) grain size in the micrometer range, (b) annealing temperature, (c) pre-dose and irradiation temperature, (d) heating rate as well as (e) the occupancy of the recombination sites. These previous detailed studies have provided strong evidence that tunneling is most likely the mechanism responsible for AF in this material [18,19,22,23]. In important recent work, Kitis et al. [20] and Polymeris et al. [3] showed that thermally assisted OSL (hereafter TA – OSL [24]) is a much more stable signal than signals measured at room temperature. These TA – OSL signals arise from much deeper traps [24] in all types of apatites including Durango, and demonstrate a much slower fading rate. TA – OSL provides an experimental way to access the luminescence signal from a number of traps that are thermally inaccessible in typical TL/OSL measurements, where all luminescent materials are heated up to a maximum of 500 °C [25].

The original LTR model [14] has been a major development in this research area, and has contributed in the understanding of tunneling phenomena in a random distribution of electron-hole pairs. The LTR model of Jain et al. [14], via the analytical equations by Kitis and Pagonis [15] has been successfully applied in descriptions of luminescence of feldspars [16,26,27], apatites [3,23], contaminated quartz [28], aluminium nitride ceramics [29], YPO_4 [30], de-proteinated tooth enamel [33], and MgB_4O_7:Dy,Na [31]. Recently, Şahiner et al., [32] have used the same model to study the dependence of conventional, post Infrared IRSL (pIR IRSL) and multi-elevated pIR IRSL (MET pIR IRSL) signals from a pure microcline K-feldspar on the stimulation temperature.

The main purpose of this work is to study experimentally the AF effect as a function of grain size, at the edge between the micro- and the nano-scale.

The specific goals of this work are:

1. To fabricate nanocrystalline powder samples of various sizes, by applying a dry ball milling process on Durango apatite.
2. To quantify the effective grain sizes of the powder samples using Scanning Electron Microscopy (SEM) techniques.
3. To compare and analyze the luminescence signals from these powder samples of different grain sizes, with emphasis on the g-factors which describe the AF.
4. To look for possible changes in the structure of Durango apatite due to prolonged ball milling, by using Fourier Transform Infrared (FTIR) spectroscopy.

2. Experimental procedure

2.1. Sample preparation & Ball milling conditions

The sample used in these experiments was a natural crystal of Durango apatite which is a nearly pure fluorapatite, having the chemical formula $Ca_{9.80}Sr_{0.02}Fe_{0.02}Ce_{0.04}(PO_4)_{5.92}(SiO_4)_{0.04}(SO_4)_{0.06}(F_{1.90}Cl_{0.16})$ [34,35] with a maximum of 3.47 wt% F and of 0.37 wt% Cl [36]. This is the same bulk material that has been previously used in similar reference fading studies [2,3,18–23].

The single piece of monocrystal was crushed gently using an agate mortar and grains of dimensions within the range 100–180 μm were obtained after dry sieving. The grains were annealed at 1000 °C for 1 h, followed by rapid cooling to room temperature; this was selected as the reference grain size fraction. This annealing treatment is necessary to empty all very deep traps, which may have been filled by the natural irradiation of the material. Previous work has shown that this annealing process does not influence the anomalous fading effect in Durango apatite [18]. Aliquots with mass of 7.5 mg each, were prepared by mounting the material on stainless-steel disks of 1 cm^2 area.

In order to achieve grains in the nano-size fractions, the sample was ball milled. Ball milling (hereafter BM) process was carried out inside a Retsch centrifugal ball mill, Pulverisette 6, Fritsch (model S 100). The milling was carried out in oxygen atmosphere, in a cylindrical stainless steel jar of 50 ml, using 7 steel balls of 10 mm diameter each and a rotation speed of 500 rpm. The apatite samples were milled for 0 (reference grain size fraction), 2, 4, 8, 12, 24 and 48 h in dry conditions. The initial ball-to-powder mass ratio was 40:1. The process was interrupted several times and some powder was taken out for examination. The ball milling conditions applied were previously described elsewhere [37]. Ball milling conditions were chosen to avoid the extensive agglomeration that is known to be a major problem for the ball milling of this material. After each BM time, all luminescence measurements were performed on cold-pressed pellets of the same mass, because the ball milled material was very brittle. Pellets were prepared by vacuum pumping, using a $5{\cdot}10^{-3}$ m cylindrical pressing die and 10^9 Pa pressure. The pressing time was 60 min while the mass of each pellet was 35 mg. For the conditions of the cold pressing, the authors could refer to Stathokostopoulos et al. [38].

2.2. Electron Microscopy

The morphology and the grain size distribution after each ball milling duration was obtained using a Jeol 840A scanning microscope with an energy-dispersive spectrometer attached (model ISIS 300; Oxford). Detailed SEM statistics have been applied to better monitor the particle size variation due to the milling process. The beam spot area was of 1 μm in diameter, the accelerating voltage was 20 kV, the beam current was 0.4 nA, the working distance was 20 mm, and the counting time was 60 s real time.

2.3. FTIR spectroscopy

Fourier Transform Infrared analysis was performed with a Bruker FTIR spectrometer, model IFS113v, operating under vacuum. The spectra were collected in the mid-IR region (spectral range between 4000 and 400 cm^{-1}), with 32 scans and a spectral resolution of 2 cm^{-1}. Potassium bromide pellets of 200 mg were prepared -with a 0.5–1% content of the produced apatite grains- and were examined in transmittance configuration. All collected spectra showed substantially low signal-to-noise ratio. All measurements of pellets were performed in the transmittance configuration; a single Durango fluorapatite crystal was also examined in reflectance mode.

2.4. Apparatus and measurement conditions for luminescence

All luminescence measurements were carried out using a Risø TL/OSL Reader (model TL/OSL–DA–20), equipped with a high power blue LED light source (470 nm, FWHM 20 nm) and a $^{90}Sr/^{90}Y$ beta particle source, delivering a nominal dose rate of 0.1083 Gy/s [39]. A 9635QB photomultiplier tube with a Hoya (U-340) blue filter was used for light detection (340 nm, FWHM 80 nm). All TL measurements and heatings were performed in a nitrogen atmosphere with a low constant heating rate of 1 °C/s, to avoid significant temperature lag between the sample heater and the top surface of the sample [40]; TL measurements were performed up to the maximum temperature of 500 °C. The OSL stimulation wavelength is (470 ± 20) nm for the case of blue stimulation, delivering at the sample position a maximum power of 40 mW/cm^2. Both conventional OSL as well as TA – OSL measurements were performed in the continuous wave configuration (CW-OSL), with the power level being software controlled and set at 90% of the maximum stimulation intensity for blue LEDs. TA – OSL was measured according to the protocol suggested by Polymeris et al. [41,42]; the optimum temperature for the OSL measurement that was determined and adopted by Polymeris et al. [3] as well as by Kitis et al. [20] has been used, namely 200 °C.

2.5. Experimental Protocols

In order to check whether a sample yields anomalous fading, a standard test includes taking measurements of the corresponding luminescence signal immediately (promptly) after an irradiation in the laboratory, and at some later times. A series of such measurements are undertaken to plot the luminescence output as a function of storage or fading time [1–3]. The protocol that was applied in the framework of the present study is the same as used by Polymeris et al. [3], consisting of the following steps:

Step 0: Test Dose and subsequent TL measurement to obtain the initial sensitivity.
Step 1: Test Dose, 21.5 Gy.
Step 2: Storage in dark for duration $t_i = 0$ min
Step 3: CW-OSL for 1 s at room temperature.
Step 4: Remnant TL (*R-TL* hereafter) measurement up to 500 °C.
Step 5: Increase and hold temperature at 200 °C; measure CW-OSL at this temperature for 500 s to obtain the TA – OSL signal.
Step 6: Residual TL after TA – OSL (*RTL* hereafter) measurements to check whether some phototransferred signal did not give rise to a new TA – OSL signal.
Step 7: Repeat steps 1–6 for 12 different storage times t_i, ranging up to 900 min.
Step 8: As in step 0, to obtain the final sensitivity.

The aim of step 4 is twofold: it measures the faded TL signal, and also empties all electron traps thermally activated below 500 °C. This protocol was applied in single aliquot/pellet mode for all grain sizes. According to our previous studies, Durango apatite does not show significant sensitivity changes following successive cycles of irradiation and TL measurements. Nevertheless, sensitivity variation tests were carried out in step 6 of the protocol. The TL glow-curves obtained from steps 0 and 6, showed a reproducibility better that 1%, implying that there is no need for sensitivity corrections [2,3,18,20]. After each TL measurement, a pause of 60 s was incorporated, to ensure that the temperature of the hot plate has decreased to room temperature. For each type of luminescence signal and storage time, a background measurement was performed, and during the data analysis this background was subtracted from the corresponding measurement.

3. Method of analysis

3.1. Expressions for anomalous fading rates (g-factors)

In this section we present the equations used to quantify the AF in the experiments. Two equations were used to quantify the AF in the experiments: the first one is based on a direct measurement of remnant luminescence signals, and the second is based on component analysis of the OSL and TA – OSL signals.

The TL, OSL and TA – OSL signals monitored during the current experiments are the *remnant luminescene signals,* i.e. the signals remaining after various times have elapsed after the end of irradiation. These remnant signals are defined as the ratio of the luminescence signal remaining after storage time t, over the corresponding signal measured at a given zero time, t_0. The equation describing these remnant luminescence signals is [2,10,43]:

$$\frac{L}{L_0} = 1-\frac{g}{100}\cdot log_{10}\frac{t}{t_0}, \quad (1)$$

where L_0 represents the first (prompt) measured luminescence signal at zero time, t_0 is the elapsed time after the end of irradiation and L the signal remaining after storage time t. Eq. (1) gives directly the value of g-factor which describes the luminescence signal loss in terms of percentage per decade of time. The elapsed time in our experiments includes a minimum time of 120 s between the end of the irradiation and the following luminescence measurement. The storage time also includes part of the irradiation time (100 s), while for TA – OSL the storage time also includes the 500 s duration of the readout. Consequently, all corresponding durations are added to the storage time sequence of step 2 [3,44,45].

In the present work an additional expression will be used, which was derived by Kitis and Pagonis [46], based on the LTR model by Jain et al. [14]. This specific expression is:

$$\frac{L}{L_0} = \exp(-12.167\cdot\rho'\cdot[log_{10}(s\cdot t)^3]) \quad (2)$$

where ρ' is a dimensionless parameter representing the concentration of the luminescence centers and s represents the frequency factor characterizing the tunneling process [46]. Eq. (2) does not yield directly the value of the g-factor as in the case of Eq. (1), so Pagonis and Kitis [46] correlated the dimensionless parameters ρ' from Eq. (2) with the g-factor of Eq. (1) by suggesting the following expression:

$$g_{50} = 2.7035\cdot\rho'^{1/3} \quad (3)$$

It must be noted that the g_{50}-factor in Eq. (3) differs from the g-factor of Eq. (1), since the former represents the g-factor when the luminescence signal has been reduced at 50% of its prompt value after the end of irradiation. However, as it was shown by Pagonis and Kitis [46], in most cases the g_{50}-factor values and the g-factor values do not differ substantially. In the framework of the present study, fading rate values will be evaluated for all three luminescence signals and for each grain size fraction, when possible, via the calculation of g_{50} and g-factors.

3.2. Expressions for the CW-OSL and TA – OSL curves

In this section we present the equations used to analyze the luminescence signals in this paper. Two equations were used to analyze the luminescence signals, based on either delocalized transitions involving the conduction band, or on localized transitions within the LTR model [14].

The CW-OSL decay curves are measured with blue light, and it was decided to analyze them using the *delocalized* analytical solutions of the one trap one recombination center (OTOR) model. Kitis and Vlachos [47] showed that the system of differential equations in the OTOR model can be solved analytically using the Lambert function $W(z)$. The solution of the OTOR model derived by Kitis and Vlachos [47] is:

$$I(T) = \frac{N\cdot R}{(1-R)^2}\cdot\frac{p(t,T)}{W(z)+W(z)^2} \quad (4)$$

where N is the total concentration of trapping states and $W(z)$ is the Lambert W function [48], and $R=A_n/A_m$ with A_n, A_m being the retrapping and recombination coefficients correspondingly. In the present work Eq. (4) will be used considering only the case $R < 1$ [47–49]. The function $p(t, T)$ in Eq. (4) concerns the stimulation mode used during the experiments. For the case of CW-OSL signals, $p(t,T) = \lambda$, and the argument z of the Lambert function $W(z)$ becomes:

$$z = \exp\left(\frac{R}{1-R} - \ln\left(\frac{1-R}{R}\right) + \frac{\lambda t}{(1-R)}\right) \quad (5)$$

In addition to Eq. (4) which is based on *delocalized* transitions, in this paper we use analytical expressions from the *localized* LTR model of Jain et al. [14]. OSL and TA – OSL signals were fitted according to the equations suggested by Kitis and Pagonis [15]:

$$I(t) = \frac{3n_0\rho' z F(t)^2}{1+z\frac{t}{\tau}}e^{-\rho' F(t)^3} \quad (6)$$

$$F(t) = ln(1+z\frac{t}{\tau}) \quad (7)$$

The free fitting parameters of Eqs. 6 and 7 are the tunneling luminescence lifetime parameter $\tau = 1/\lambda$ and the dimensionless density

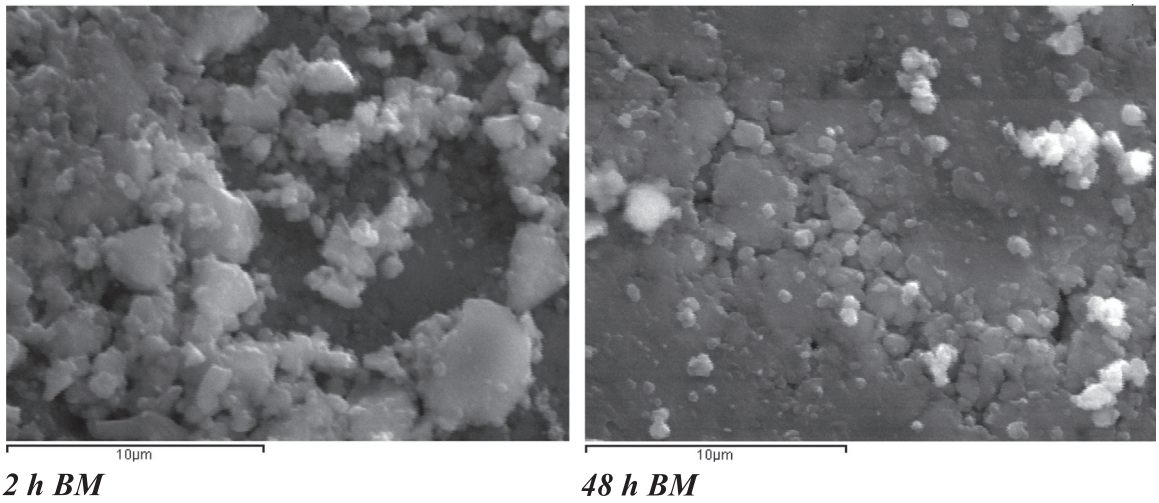

Fig. 1. SEM backscattered images of ball milled Durango apatite after 2 h (left) and 48 h (right) ball milling.

parameter ρ′. In order to describe accurately the behavior of the OSL signals at time $t = 0$, Eq. (7) was used in the empirical modified form $F(t) = ln(e+z\frac{t}{\tau})$. This empirical correction is based on the requirement that the intensity of the normalized Eq. (6) should be unity for $t = 0$.

The ROOT data Analysis Framework was used [50], while all fittings were performed using the MINUIT program [51] released in ROOT, which is a physics analysis tool for function minimization. The Lambert function $W(z)$ is implemented in ROOT through the GNU scientific library (GNU GSL) [52]. The goodness of fit was tested using the Figure Of Merit (FOM) [53] given by:

$$FOM\,(\%) = 100 * \sum_{p} |TL_{exp} - TL_{fit}| / \sum_{p} TL_{fit} \quad (8)$$

The FOM index value provides a measure for the goodness of fit; the lower its value, the better the quality of the fit.

4. Results and discussion

4.1. Ball milling procedure and grain size fractions

Fig. 1 shows two SEM backscattered images corresponding to BM durations of 2 and 48 h respectively. Note that both SEM images are presented at the same scale for the sake of comparison. This figure shows clearly that the grains in the case of the 2 h BM process are quite large, but they are still in the range of few micrometers. The second image with the BM duration of 48 h indicates much smaller grains. The SEM images were quantified by using image analysis, with the results shown in Fig. 2.

Fig. 2**a** shows the distributions of grain sizes and their corresponding dependence on the BM duration. The inset indicates the distribution of the grain sizes without any ball milling, after gently crushing the crystalline apatite using an agate mortar. Each distribution was fitted using a Gaussian distribution function. The position of the center of the peak represents the average grain size, and the Gaussian Root Mean Square (RMS hereafter) width corresponds to the standard deviation. As the BM duration becomes more prolonged, the distributions shift to smaller grain sizes. For BM durations up to 24 h, the distributions are quite narrow; however, BM for 48 h results in lower grain size fraction, in conjunction with a much wider distribution of grain sizes. The inset of Fig. 2**a** verified that when no balling is applied, the resulting grains are in the range 100–180 μm. It is worth mentioning that, by increasing the BM duration further than 48 h, only the Gaussian RMS width, thus the standard deviation changes; the centroid is almost the same. This latter feature could be due to the extensive agglomeration that is known to be a major problem for the prolonged ball milling of this material, because the ball milled material is very brittle. This is the reason why the present study is limited to BM durations up to 48 h.

Fig. 2**b** shows the dependence of the average grain size on the BM time, with the dashed line providing a guide to the eye. For short BM times of 2 h and 4 h, the average grain size fraction is still of the order of few μm. As the ball milling duration increases further, the average grain size fraction becomes of the order of hundreds of nm. The lowest grain sizes were achieved after 48 h of BM, and are around 200 nm; nevertheless, as the corresponding distributions showed, much smaller grains also co-exist with these much larger grains.

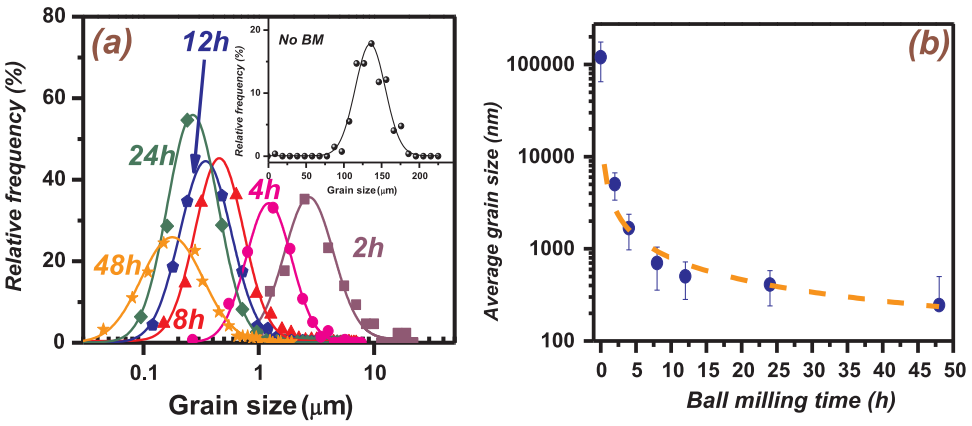

Fig. 2. Plot (a) presents the grain size distribution for different ball milling durations. The inset shows the distribution for the powder without ball milling. Plot (b) presents grain size versus the ball milling duration in terms of the centroid of each distribution presented in plot (a). Errors are expressed as 1σ. The dashed line provides a guide for the eye.

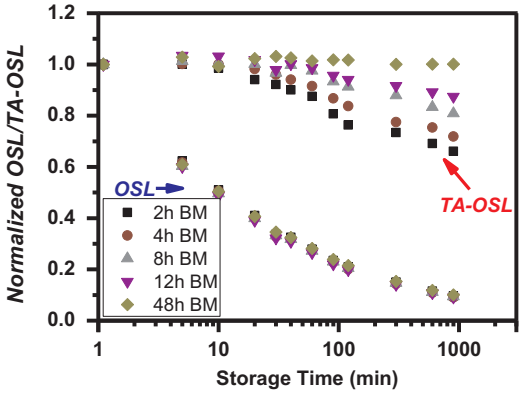

Fig. 3. Normalized residual OSL and TA – OSL output as a function of storage time for various ball milling times.

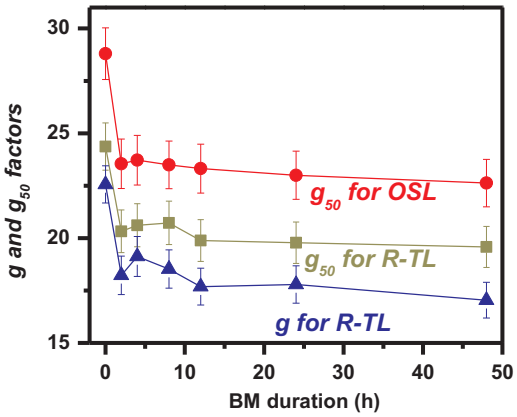

Fig. 5. g and g_{50} factors versus BM durations. The g factors were evaluated according to Eq. (1) using the integrated luminescence intensity; an example of the corresponding analysis is presented in Fig. 4a. The g_{50} factors were evaluated by using Eq. (3), after evaluating ρ′ according to Eq. (2), using the integrated luminescence intensity; an example of the corresponding analysis is presented in Fig. 4b.

4.2. Anomalous fading rate based on the integrated TL, OSL and TA – OSL signals

The analytical expressions of Section 3.1 were used to obtain the values of the g-factors for the different grain size samples.

The present study shows AF effects are ubiquitous for both TL and OSL signals, and for all grain size fractions studied in this paper. This is in agreement with the recent report by Polymeris et al. [3] that AF effect is always present in TL/OSL signals of many apatite samples, with grain sizes between 80 and 140 μm.

Fig. 3 shows plots of normalized luminescence output versus storage time, for both conventional OSL and TA – OSL integrated signals. The AF rate of integrated OSL is the same for all grain sizes between 5 μm and 200 nm (correspoding to 2 and 48 h BM respectively). Strong anomalous fading was also monitored for the case of TL (not shown here), without substantial variation in the fading rate over the various BM durations. However, the TA – OSL signals in Fig. 3 appear to be much more stable compared to both OSL and TL signals, in full agreement with previously reported results [3,20]. Most importantly, Fig. 3 shows that the AF rate for TA – OSL signals depends clearly on the grain size; as the grain size decreases, the AF rate decreases. At grain sizes resulting from the 24 and 48 h BM (average grain size 350 and 200 nm correspondingly), the AF is almost negligible. For small BM times of 2 and 4 h, the largest calculated g-factor was of the order of 4–6%.

Normalized plots of the integrated R-TL signals versus storage times were fitted using both Eq. (1) and Eq. (2). Fig. 4**a** shows a typical example of fitting the integrated R-TL for 8 h of BM using Eq. (1), with the g-factor evaluated directly from the fitting procedure. Fig. 4**b** shows an example of fitting the R-TL and R-CW-OSL signals using Eq. (2). The fitting procedure using Eq. (2) results in the value of the fitting parameter ρ′, from which the value of the g_{50} is next obtained using Eq. (3).

Fig. 5 shows the values of the *g* or g_{50} factors obtained using these two fitting procedures, as a function of the BM duration. This figure shows that the g-factor values for samples which did not undergo the BM procedure (i.e. BM time = zero h), is very high and in the range g = 22–28. As the BM time increases, the g-factor drops significantly even for a short BM time of 2 h. Subsequent increase of the BM time in the range 4–48 h causes a small decrease of the g-factors. In a previous study, Kitis et al. [18] have pointed out that TL AF rates do not show variation versus the grain size in the micrometer range; however, their finest grain size included 10 μm. It seems that as the grains become smaller than 10 μm, there is a steep decrease of the AF rate. It is also noted that the g_{50} factor evaluated indirectly through Eq. (3) are in very good agreement with the *g-factor* evaluated directly from Eq. (1).

4.3. Anomalous fading rate as a function of R-TL glow-curve temperature

In this section we study the AF factor as a function of the temperature along the TL glow curve. Previous work by Bowman [54] and Polymeris et al., [2,3] showed that the g-factor can vary for different parts of the TL glow curve, and this effect could be possibly attributed to thermally assisted tunneling [9].

On the basis of these previous studies, we attempted a differential TL glow curve analysis, towards investigating possible dependence of the AF rate on the temperature along the glow curve. Fig. 6 shows two typical TL glow curves for Durango apatite, one corresponding to a measurement immediately after irradiation (prompt curve), and one after storage of 300 min, and for two different BM times. For all grain size fractions studied in this paper, the glow-curve shape remained the

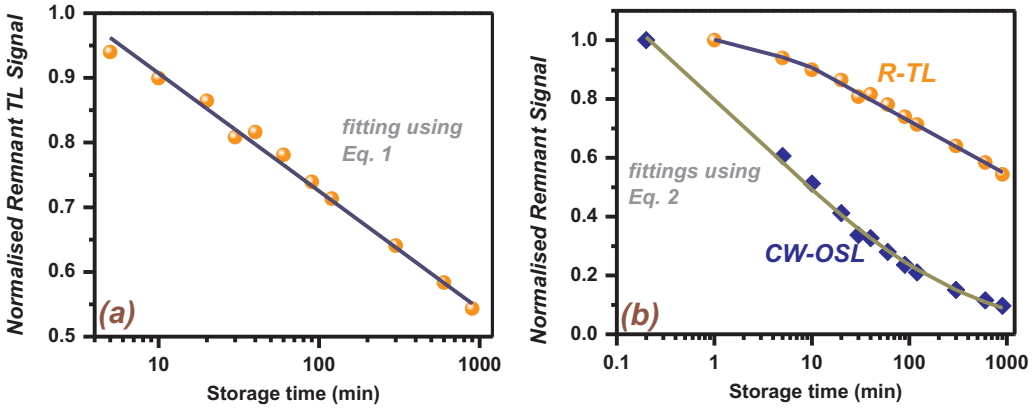

Fig. 4. Fitting examples of (a) normalized R-TL as a function of storage time using Eq. (1). and (b) normalized R-TL and residual OSL as a function of storage time using Eq. (2).

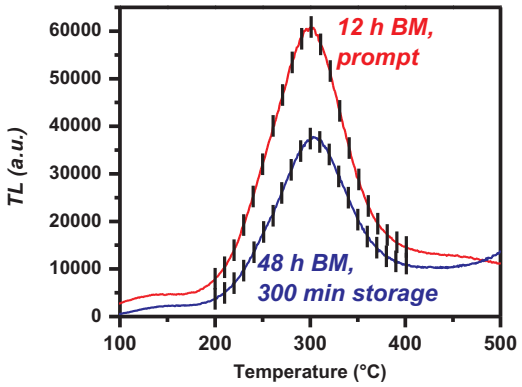

Fig. 6. TL glow-curves of Durango apatite for (a) prompt measurement after 12 h BM and (b) for storage time of 300 min corresponding to 48 h BM. The vertical bars on the glow curves show the temperatures T_i from which TL integrations over 10 °C occur, to evaluate the AF rate as a function of the glow curve temperature.

same, consisting of several overlaping TL peaks [2,3,18–23], and was not affected by the intense AF phenomena described in the previous section.

The procedure followed in the differential TL glow curve analysis was as follows. Sections of the TL glow curves within a temperature interval of $\Delta T = 10$ °C were selected, and within the range 200–400 °C; these temperature intervals are shown by vertical lines in Fig. 6. The integrated intensity for each temperature interval $T_i + \Delta T = T_i + 10$ °C is plotted as a function of the storage time, similar to the plots shown in Fig. 4. These plots were then analyzed by using both Eq. (1) and Eqs. 2–3. In this manner the g-factor is obtained for each of these intervals of width $\Delta T = 10$ °C. A total of 182 plots of R-TL versus storage time were analyzed for the various grain size fractions.

The basic fitting parameter obtained from Eqs. 2–3 is the value of the parameter ρ′, which is shown for all grain sizes in Fig. 7. This figure reveals two extremely interesting experimental features: (a) There is a mild but clear decrease of the ρ′ values as a function of the glow-curve temperature up to 400 °C, and for all grain size fractions, and (b) for the same temperature interval $T_i + 10$ °C, there is a mild differentiation on the values of the ρ′ parameter from the grain size corresponding to 2 h BM up to the grain size corresponding to 48 h BM.

Fig. 8**a** shows the *g*-factor as a function of the glow-curve temperature using Eq. (1), while Fig. 8**b** shows the g_{50} factor evaluated using the ρ′ values of Fig. 7 and Eq. (3). For all grain size fractions, the AF rate decreases with increasing temperature along the TL glow curve. These results are in good agreement with the work by Polymeris et al. [2]. Finally, the g_{50} and *g*-factors from Figs. 8**a** and 8**b** are almost identical up to a glow-curve temperature of 300 °C, with a slight deviation coccurring between the two g-factors seen above 300 °C.

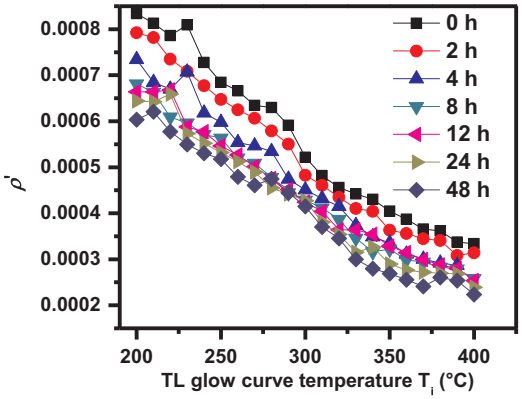

Fig. 7. The dependence of the dimensionless parameter ρ′ evaluated from the fitting procedure using Eq. (2), on the glow-curve temperature for various grain sizes.

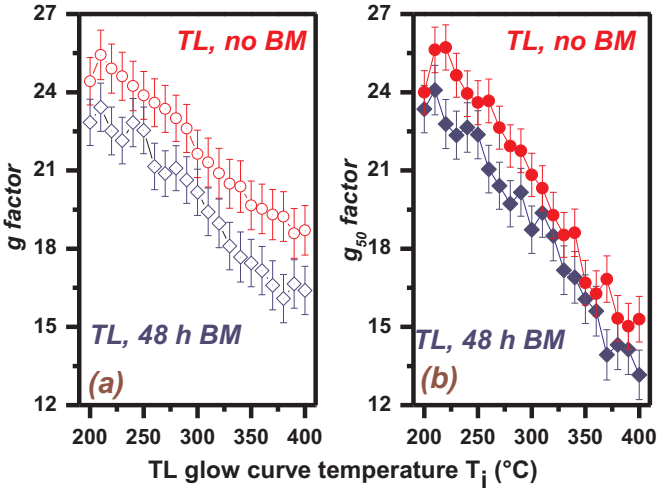

Fig. 8. Plot (a) depicts the values of the g-factor evaluated from the fitting according to Eq. (1), as a function of the glow-curve temperature for ball milling durations 0 and 48 h. Plot (b) presents the values of the g_{50} factors, evaluated from the ρ′ values of Fig. 7 using Eq. (3) for ball milling durations 0 and 48 h versus the glow curve temperature. The behavior of all other ball milling durations lies between that of 0 and 48 h of BM.

4.4. Analysis of CW-OSL decay curves

The experimental protocol of the present work includes CW-OSL measurements for stimulation duration of 1 s; in fact this is a common practice in OSL measurement protocols. In the present study, the intensity of the CW-OSL signal during this initial stimulation was very high; therefore it was decided to set a very small sampling time of 1 ms, with every CW-OSL measurement consisting of 1000 data points.

We have attempted to fit the short CW-OSL signals using the analytical tunneling Eqs. 6 and 7. It was found that Eq. (6) gives excellent fits to the experimental CW-OSL decay curves of 1 s, by using a *single component*. A fitting example of the CW-OSL using Eqs. 6 and 7 is presented in Fig. 9. Although the value of ρ′ could not be obtained reliably from these fits, Fig. 10 shows the dependence of the tunneling lifetime parameter τ on the storage time, for two different ball milling durations of 2 h and 48 h. The rest of the experimental values of τ obtained for different BM times are not shown for clarity, but they lie essentially in-between the two curves in Fig. 10. This latter figure shows that the tunneling lifetime τ increases systematically with the storage time, and its value also depends on the grain size. This increase of the τ parameter with storage time can be interpreted within the LTR model, as follows. As the storage time is increased, pairs of electrons and positive charges corresponding to shorter distances recombine first, and

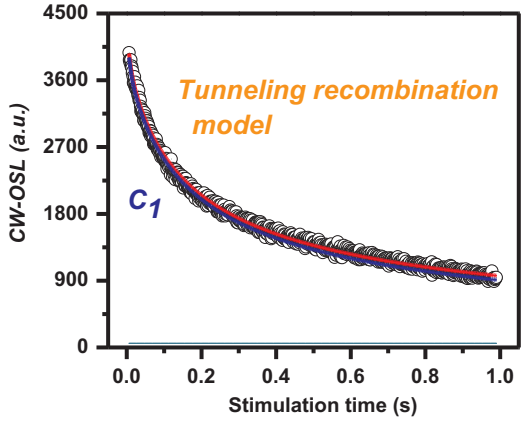

Fig. 9. CW-OSL curve, analyzed using the tunneling recombination expressions according to Eqs. 6 and 7.

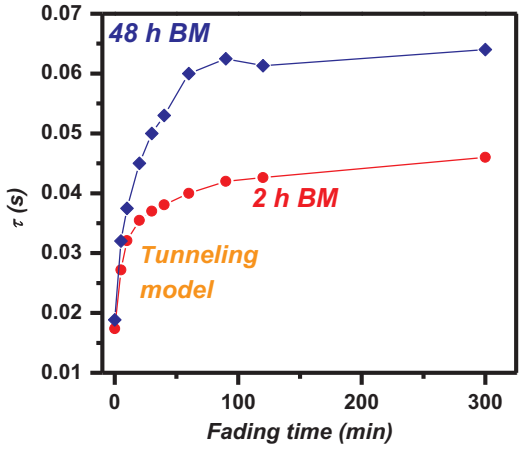

Fig. 10. The behavior of the mean tunneling recombination lifetime for the unique component of the OSL signal, for ball milling durations of 2 and 48 h, as a function of storage time. The behavior of all other grain sizes is between that of 2 and 48 h BM.

only more distant pairs remain in the system, leading to an increase of effective the lifetime τ. These results are also discussed in Section 5.

4.5. Analysis of TA – OSL decay curves

The TA – OSL decay curves were analyzed using a linear combination of a localized and a delocalized transition. The shapes of all TA – OSL curves yield a monotonic decay similar to the shapes of conventional CW-OSL signals. Since the TA – OSL is measured using blue stimulation with photon energies of ~2.4 eV, one might expect the presence of a strong delocalized component in these signals. Therefore, we assume that the TA – OSL emission of Durango apatite can be described by a superposition of two components, a *delocalized* OTOR component described by Eqs. 4 and 5, and a *localized* tunneling component described by Eqs. 6 and 7. The results of this analysis can be summarized as follows.

Fig. 11 shows the luminescence lifetime τ of the *tunneling* component for each grain size fraction, as a function of fading time. The value of this tunneling lifetime increases at short fading storage times, and reaches a plateau for the more prolonged storage times. In addition, longer BM times result in higher values for the tunneling lifetime of the TA – OSL signal. The overall values of this tunneling lifetime are in the range 4–8 s. The value of the lifetime parameter τ corresponds to the time required for recombination, indicating also the distance that the

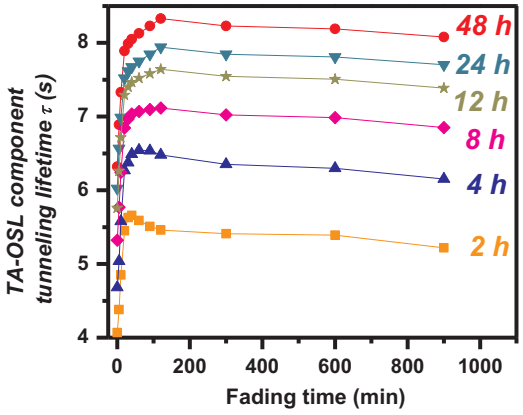

Fig. 11. The behavior of the mean tunneling recombination lifetime of the first component of the TA – OSL for all ball milling durations (2–48 h) as a function of the fading storage time. For the other component of the TA – OSL signal, the OTOR model was used, according to Eqs. 4 and 5; the corresponding lifetime is stable, independent on both ball milling and fading times.

electron travels before recombination, explaining thus why the value of the τ parameter for the tunneling recombination component starts to increase, reaching a final stable value. According to Figs. 10 and 11, as the grain size fraction decreases, the time required for the tunneling recombination becomes longer for both OSL and TA – OSL. A careful comparison between these two figures indicates that the tunneling recombination lifetime parameter τ for the case of TA – OSL becomes at least 200 times larger than the corresponding of the OSL. As the applied protocol includes TA – OSL measurement after both OSL and TL measurements, it is safe to conclude that prior OSL and TL measurements consume effectively the distant pairs of donors and acceptors and therefore the subsequent TA – OSL signal shows almost no anomalous fading. This explains why the lifetimes of the OSL signals are much shorter than the corresponding lifetimes of the TA – OSL signals.

The luminescence lifetime of the *delocalized* component (not shown as a graph here) is much larger with a value around 300 s, and is independent of both the fading storage time and of the grain size fraction.

During the fading storage time, the most proximal pairs are consumed by both radiative and non-radiative recombinations. OSL measurement follows directly after storage, sweeping the residual most distant recombination pairs of donnors and acceptors; this is the reason why the fading for the case of OSL is the most intense. In between OSL and TA – OSL, the TL measurement takes place, with the TL signals indicating intense fading rates as well, even though somewhat milder when compared to the AF rates of OSL signals. This latter experimental fact indicates that TL consumes even more increasingly distant pairs, compared to the case of OSL. A subsequent (TA –) OSL measurement at elevated temperature is able to access a greater volume of the crystal, thus being able to access more distant holes. This is the reason why TA – OSL shows negligible fading.

4.6. FTIR analysis

In this section we present experimental FTIR results, which test whether any physical changes occur in the Durango apatite samples due to the ball milling procedures.

The infrared spectra of the apatite crystal are shown in Fig. 12**,** with Fig. 12**a** depicting a reference spectrum in the reflectance mode from a single crystal.

Fig. 12**b** shows the spectra in the transmittance mode corresponding to various ball-milling durations, along with that corresponding to the initial coarse grains. The sharp band at 1095 cm^{-1}, the shoulder at 1075 cm^{-1} and the sharp band at 1040 cm^{-1} are all attributed to the ν_3 assignments of the antisymmetric stretching of P-O bonds of the PO_4^{3-} ion [55]. The band at 960 cm^{-1} corresponds to the ν_1 symmetric stretch of the PO_4^{3-} ion, the weak band at 870 cm^{-1} is assigned to the combination of the $\nu_4+\nu_2$ modes [55], the strong bands at 603 and 566 cm^{-1}, and the shoulder at 574 cm^{-1}, are attributed to the ν_4 bending of P-O bonds of the PO_4^{3-} ion [55]. The band at 472 cm^{-1} can be assigned to the ν_2 mode (out-of-plane bending) of the PO_4^{3-} ion [56], where it splits into two bands. The first is clearly observed at 472 cm^{-1} and the second one appears as a shoulder at 463 cm^{-1} [57]. The weak band at 520 cm^{-1} suggests the weak participation of a silicate phase [58].

In addition to the attributed mineral fluorapatite bands, as they were described above, some accessional bands appear in the spectrum of the initial coarse grains. The weak and broad band at 740 cm^{-1} and the weak and sharp band at 668 cm^{-1} introduce the presence of hydroxy-fluorapatite. Specifically, the first band shows the presence of OH…F polymerization [59] or the substitution of fluoride by OH^- ions [60] and the second one a degree of OH…F…OH polymerization [59]. Above the first four hours of BM procedure, the carbonate content of the grains begins to appear: the weak bands at 1456, 1420, 868 and 712 cm^{-1} are indicative of the detectable carbonate group, because of the OH^-, F^- or PO_4^{3-} anion substitution by CO_3^{2-} [60]. These experimental results imply the formation of $CaCO_3$ in low quantities.

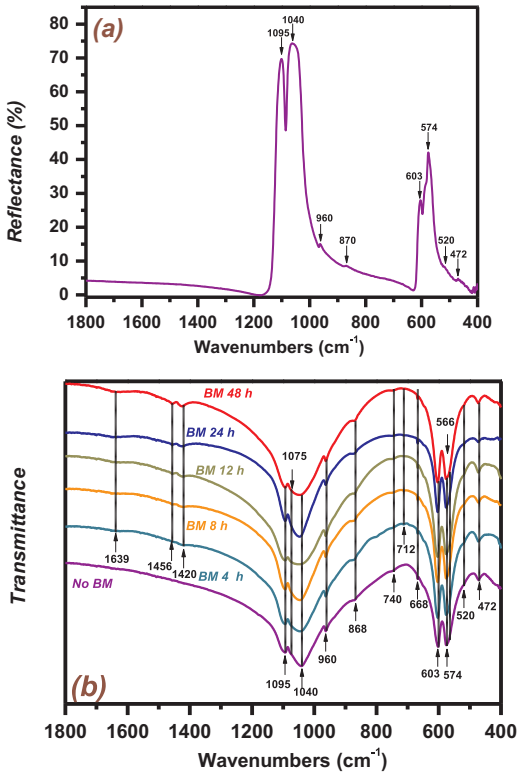

Fig. 12. FTIR spectra of (a) Durango fluorapatite single crystal in reflectance mode and (b) in transmittance mode from the initial grinded material as well as after 4, 8, 12, 24 and 48 h of ball-milling procedure. The wavenumbers of the main bands are also presented in arrows.

Nevertheless, the weak and broad band at approximately 1639 cm^{-1}, that also begins to appear in the spectra above the four hours of BM, can be assigned to the bending modes of molecular H_2O in carbonate rich fluorapatite [61]. The bands which are assigned to the carbonate and hydroxyl content have the tendency to become slightly stronger while the grain size decreases.

In summary, the FTIR analysis indicated that the ball-milling procedure does not alter the chemical structure of the apatite. This result can be also supported by the shape of the TL glow curves, which do not change with BM. The only difference that is imposed by the ball-milling procedure deals with the initial formation stages of $CaCO_3$ and hydroxy-fluorapatite; this latter feature was monitored by the FTIR analysis. Once again, as the TL glow curves do not change in shape, the quantities of the $CaCO_3$ and hydroxy-fluorapatite are insignificant, as the FTIR monitors the initial stage of the corresponding formations. Nevertheless, since AF rate differentiation is observed only for the case of TA – OSL signals, one can safely conclude that this AF cannot be attributed to the formation of $CaCO_3$, as this latter material does not yield TA – OSL signal with fast component [62].

5. Conclusions

The present work provides a new type of study of anomalous fading in Durango apatite as a function of ball milling time. SEM measurements verified that different BM durations resulted in different average grain size fractions, as low as 200 nm. The anomalous fading effect was studied for OSL, TL as well as TA – OSL signals. All grain size fractions showed AF of the TL and OSL signals. Moreover, TA – OSL signals were found to fade in a much slower rate than either the TL or the conventional OSL signals. Since TA – OSL measurements follow a TL measurement up to 500 °C, these signals emerge from deeper traps. Further work is required to identify the different defects which could be associated with those deeper traps; this study is currently in progress, including mostly Electron Paramagnetic Resonance (EPR) characterization. FTIR analysis indicated that the ball milling procedure does not induce a new phase in the crystal.

An important result from this work is that the fading rate for TL and OSL does not depend on grain size. On the contrary, the fading rate for TA – OSL signals decreases as the grain size fraction is decreased, while for grain size fractions between 200 and 450 nm the fading rate stays constant. These results seem at first to contradict what one might expect from a theoretical point of view. However, recent simulation work has confirmed that the behavior seen in our experiments is possible under the right physical conditions in the nanomaterial. Specifically Pagonis et al. [63] used Monte Carlo (MC) techniques to simulate the effect of crystal size on quantum tunneling phenomena in nanocrystals, based on a critical assumption of a random distribution of electrons and positive ions. These authors have concluded that the behavior of such random distributions is determined by three characteristic lengths: (I) the radius of the crystal R, (II) the tunneling length a, and (III) the initial average distance $\langle d \rangle$ between electrons and positive ions (which is directly related to the density of charges in the material). Due to the presence of three different parameters, the tunneling recombination rate yields a complicated dependency on the size of the nanocrystals. When the tunneling length a is much smaller than both R and $\langle d \rangle$, simulations showed that smaller crystals exhibit a faster tunneling recombination rate. However, when the tunneling length a is of the same order of magnitude as both R and $\langle d \rangle$, the opposite effect is observed, namely smaller crystals yield slower tunneling recombination rate. The rate of tunneling in both cases reaches the limit expected for bulk materials eventually, for increasing crystalline size. The experimental results presented in this paper are consistent with, and can be interpreted on the basis of these recent Monte Carlo simulations.

A differential analysis on the TL glow curves indicated a dependence of the AF rate on the glow curve temperature, within the range 200–400 °C. This AF rate decreased with increasing temperature, and with increasing BM time, suggesting the need for more complicated models which would possibly include a combination of thermally assisted tunneling, delocalized transitions involving the conduction band, and also localized transitions.

Finally, it is important to point out that the proposed component analysis of the TA – OSL decay curves was based on a linear combination of a localized and a delocalized transition. Our choice of such a linear combination is rather arbitrary, since one could also choose two tunneling components for such an analysis; however it has been effectively applied before in both cases of prompt isothermal TL of Durango apatite [23] as well as to de-proteinated tooth enamel [33]. The difference in the latter choice would be that one would be dealing with competition effects, rather than a superposition of states as in our analysis. The reason we prefer to use a linear combination of localized and delocalized components, is that the blue stimulating light has a photon energy of 2.4 eV, and this should in principle be enough to raise electrons from the ground state into the conduction band. However, this is just our working hypothesis, and further experimental work needs to be carried out, perhaps with LEDs of different stimulating wavelengths. Nevertheless, the de-convolution parameters of the present analysis provide useful insight regarding the luminescence mechanism in OSL and TA – OSL, describing thus the fading behavior of the luminescence in Durango apatite.

Acknowledgements

SEM measurements have been performed at the Solid State Physics section in Physics Department of Aristotle University (Thessaloniki-Greece) by Prof. E. Pavlidou. She is warmly thanked. Moreover, we acknowledge Prof. K.M. Paraskevopoulos for providing access to the FTIR infrastructures at the same department.

References

[1] G.A.T. Duller, Behavioural studies of stimulated luminescence from feldspars, Radiat. Meas. 27 (5–6) (1997) 663–694.
[2] G.S. Polymeris, N.C. Tsirliganis, Z. Loukou, G. Kitis, A comparative study of anomalous fading effects of TL and OSL signals of Durango apatite, Phys. Status Solidi (a) 203 (2006) 578–590.
[3] G.S. Polymeris, V. Giannoulatou, I.K. Sfampa, N.C. Tsirliganis, G. Kitis, Search for stable energy levels in materials exhibiting strong anomalous fading: the case of apatites, J. Lumin. 153 (2014) 245–251.
[4] D.J. Huntley, M. Lamothe, Ubiquity of anomalous fading in K-feldspar and the measurement and correction for it in optical dating, Can. J. Earth Sci. 38 (2001) (2001) 1093–1106.
[5] P. Morthekai, M. Jain, A.S. Murray, K.J. Thomsen, L. Bøtter-Jensen, Fading characteristics of martian analogue materials and the applicability of a correction procedure, Radiat. Meas. 43 (2008) 672–678.
[6] J.P. Buylaert, A.S. Murray, K.J. Thomsen, M. Jain, Testing the potential of an elevated temperature IRSL signal from K-feldspar, Radiat. Meas. 44 (2009) 560–565.
[7] M. Jain, C. Ankjaergaard, Towards a non-fading signal in feldspars: inside into the charge transport and tunneling from time-resolved optically stimulated luminescence, Radiat. Meas. 46 (2011) 292–309.
[8] R. Visocekas, N.A. Spooner, A. Zink, P. Blanc, Tunnel afterglow, fading and infrared emission in thermoluminescence of feldspars, Radiat. Meas. 23 (1994) 377–385.
[9] R. Visocekas, T. Ceva, C. Marti, F. Lafaucheux, M.C. Roberts, Tunneling radiative recombination in labradorite: its association with anomalous fading in thermoluminescence, Phys. Status Solidi (a) 35 (1976) 315–327.
[10] R. Chen, S.W.S. McKeever, Theory of Thermoluminescence and Related Phenomena, World Scientific, Singapore, 1997.
[11] A.G. Wintle, Anomalous fading of thermo-luminescence in mineral samples, Nature 245 (1973) 143–144.
[12] A.G. Wintle, Detailed study of minerals exhibiting anomalous fading, J. Lumin. 15 (1977) 385–393.
[13] N.R.J. Poolton, R.H. Kars, J. Wallinga, A.J.J. Bos, Direct evidence for the participation of band-tails and excited-state tunnelling in the luminescence of irradiated feldspars, J. Phys. Condens. Matter 21 (2009) 485505.
[14] M. Jain, B. Guralnik, M.T. Andersen, Stimulated luminescence emission from localized recombination in randomly distributed defects, J. Phys. Condens. Matter 24 (2012) 385402.
[15] G. Kitis, V. Pagonis, Analytical solutions for stimulated luminescence emission from tunneling recombination in random distributions of defects, J. Lumin. 137 (2013) 109–115.
[16] V. Pagonis, H. Phan, D. Ruth, G. G. Kitis, Further investigations of tunnelling recombination processes in random distributions of defects, Radiat. Meas. 58 (2013) 66–74.
[17] M. Jain, R. Sohbati, B. Guralnik, A.S. Murray, M. Kook, T. Lapp, A.K. Prasad, K.J. Thomsen, J.P. Buylaert, Kinetics of infrared stimulated luminescence from feldspars, Radiat. Meas. 81 (2015) (2015) 242–250.
[18] G. Kitis, P. Bousbouras, C. Antypas, S. Charalambous, Anomalous fading in apatite, Nucl. Tracks Radiat. Meas. 18 (1991) 61–65.
[19] G. Kitis, G.S. Polymeris, V. Pagonis, N.C. Tsirliganis, Thermoluminescence response and apparent anomalous fading-factor of Durango fluorapatite as a function of the heating rate, Phys. Status Solidi (a) 203 (2006) 3816–3823.
[20] G. Kitis, G.S. Polymeris, V. Pagonis, N.C. Tsirliganis, Anomalous fading of OSL signals originating from very deep traps in Durango apatite, Radiat. Meas. 49 (2013) 73–81.
[21] N.C. Tsirliganis, G.S. Polymeris, Z. Loukou, G. Kitis, Anomalous fading of the TL, Blue-SL and IR-SL signals of fluorapatite, Radiat. Meas. 41 (2006) 954–960.
[22] N.C. Tsirliganis, G.S. Polymeris, G. Kitis, V. Pagonis, Dependence of the anomalous fading of the TL and blue OSL of fluorapatite on the occupancy of the tunnelling recombination sites, J. Lumin. 126 (2007) 303–308.
[23] I.K. Sfampa, G.S. Polymeris, N.C. Tsirliganis, V. Pagonis, G. Kitis, Prompt isothermal decay of thermoluminescence in an apatite exhibiting strong anomalous fading, Nucl. Instrum. Methods Phys. Res. Sect. B Beam Interact. Mater. At. 320 (2014) 57–63.
[24] G.S. Polymeris, Thermally assisted OSL (TA – OSL) from various luminescence phosphors; an overview, Radiat. Meas. 90 (2016) 145–152.
[25] A.N. Nyirenda, M.L. Chithambo, G.S. Polymeris, On luminescence stimulated from deep traps in a-Al_2O_3:C, Radiat. Meas. 90 (2016) 109–112.
[26] V. Pagonis, M. Jain, K.J. Thomsen, A.S. Murray, On the shape of continuous wave infrared stimulated luminescence signals from feldspars: a case study, J. Lumin. 153 (2014) 96–103.
[27] I.K. Sfampa, G.S. Polymeris, V. Pagonis, E. Theodosoglou, N.C. Tsirliganis, G. Kitis, Correlation of basic TL, OSL and IRSL properties of ten K-feldspar samples of various origins, Nucl. Instrum. Methods Phys. Res. B 359 (2015) 89–98.
[28] E. Şahiner, N. Meriç, G.S. G.S. Polymeris, Assessing the impact of IR stimulation at increasing temperatures to the OSL signal of contaminated quartz, Radiat. Meas. 68 (2014) 14–22.
[29] L. Trinkler, B. Berzina, Localised transitions in luminescence of AlN ceramics, Radiat. Meas. 71 (2014) 232–236.
[30] A. Dobrowolska, A.J.J. Bos, P. Dorenbos, Electron tunnelling phenomena in YPO4: ce,ln (Ln ≡ Er, Ho, Nd, Dy), J. Phys. D Appl. Phys. 47 (2014) 335301.
[31] G. Kitis, G.S. Polymeris, I.K. Sfampa, M. Prokic, N. Meric, V. Pagonis, Prompt isothermal decay of thermoluminescence in MgB_4O_7:dy,na and LiB_4O_7:cu,in dosimeters, Radiat. Meas. 84 (2016) (2016) 15–25.
[32] E. Şahiner, G. Kitis, V. Pagonis, N. Meriç, G.S. G.S. Polymeris, Tunnelling recombination in conventional, post-infrared and post-infrared multi-elevated temperature IRSL signals in microcline K-feldspar, J. Lumin 188 (2017) (2017) 514–523.
[33] N. Meriç, U.R. Yuce, E. Şahiner, A. Damianidis, G.S. Polymeris, Dose response and fading studies on de-proteinated tooth enamel after de-convolution using the sum of general order kinetics and a component for tunnelling recombination, Radiat. Meas. 81 (2015) (2015) 257–261.
[34] E. Young, A. Myers, E. Munson, N. Conklin. Mineralogy and geochemistry of fluorapatite from Cerro de Mercado, Durango, Mexico. U.S. Geological Survey Professional Paper, Vols. 650-D, 1969, pp. D84-D93.
[35] J. Hughes, M. Cameron, K. Crowley, Structural variations in natural F, OH, and Cl apatites, Am. Mineral. 74 (1989) 870–876.
[36] R. Siddall, A. A. Hurford, Semi-quantitative determination of apatite anion composition for fission-track analysis using infra-red microspectroscopy, Chem. Geol. 150 (1998) 181–190.
[37] M. Ioannou, E. Hatzikraniotis, Ch Lioutas, Th Th. Hassapis, K.M. Paraskevopoulos Altantzis, Th Th. Kyratsi, Fabrication of nanocrystalline Mg_2Si via ball milling process: structural studies, Powder Technol. 217 (2012) (2012) 523–532.
[38] D. Stathokostopoulos, D. Chaliampalias, E. Tarani, A. Theodorakakos, V. Giannoulatou, G.S. Polymeris, E. Pavlidou, K. Chrissafis, E. Hatzikraniotis, K.M. Paraskevopoulos, G. Vourlias, Formation of the thermoelectric candidate chromium silicide by use of a pack-cementation process, J. Electron. Mater. 43 (10) (2014) 3733–3739.
[39] L. Bøtter-Jensen, E. Bulur, G.A.T. Duller, A.S. Murray, Advances in luminescence instrument systems, Radiat. Meas. 32 (2000) 523–528.
[40] G. Kitis, N.G. Kiyak, G.S. Polymeris, Temperature lags of luminescence measurements in a commercial luminescence reader, Nucl. Instrum. Methods Phys. Res. B 359 (2015) 60–63.
[41] G.S. Polymeris, S. Raptis, D. Afouxenidis, N.C. Tsirliganis, G. Kitis, Thermally assisted OSL from deep traps in Al_2O_3:C, Radiat. Meas. 45 (2010) 519–522.
[42] G.S. Polymeris, E. Şahiner, N. Meriç, G. Kitis, Experimental features of natural thermally assisted OSL (NTA – OSL) signal in various quartz samples; preliminary results, Nucl. Instrum. Methods Phys. Res. B 349 (2015) 24–30.
[43] B. Li, S.-H. Li, The effect of band-tail states on the thermal stability of the infrared stimulated luminescence from K-feldspar, J. Lumin. 136 (2013) 5–14.
[44] M.J. Aitken, An Introduction to Optical Dating, Oxford University Press, 1998.
[45] M. Auclair, M. Lamothe, S. Huot, Radiat. Meas. 37 (4–5) (2003) 487.
[46] V. Pagonis, G. Kitis, Mathematical aspects of ground state tunnelling models in luminescence materials, J. Lumin. 168 (2015) 137–144.
[47] G. Kitis, N.D. Vlachos, General semi-analytical expressions for TL, OSL and other luminescence stimulation modes derived from the OTOR model using the Lambert W-function, Radiat. Meas. 48 (2012) 47–54.
[48] R.M. Corless, G.H. Gonnet, D.G.E. Hare, D.J. Jeffrey, D.E. Knuth, On the Lambert W function, Adv. Comput. Math. 5 (1996) 329–359.
[49] A.M. Sadek, H.M. Eissa, A.M. Basha, G. Kitis, Resolving the limitation of the peak fitting and peak shape methods in the determination of the activation energy of thermoluminescence glow peaks, J. Lumin. 146 (2014) 418–423.
[50] ROOT, A Data Analysis Framework. ⟨https://root.cern.ch⟩, 2015.
[51] MINUIT, a Physics Analysis Tool for Function Minimization. Released in ROOT, 2015.
[52] GSL-GNU Scientific Library; ⟨www.gnu.org/software/gsl⟩.
[53] H.G. Balian, N.W. Eddy, Figure Of Merit (FOM): an improved criterion over the normalized chi-square test for assign the goodness-of-fit of gamma ray spectral peaks, Nucl. Instrum. Method 145 (1977) 389–395.
[54] S.G.E. Bowman, Nucl. Tracks Radiat. Meas. 14 (1988) 131.
[55] C. Baddiel, E. Berry, Spectra structure correlations in hydroxy and fluorapatite, Spectrochim. Acta 22 (1966) 1407–1416.
[56] B. Fowler, "Infrared spectra of apatites," in International symposium on structural properties of hydroxyapatite and related compounds, Gaithersburg, Maryland, 1968.
[57] J. Shi, A. Klocke, M. Zhang, U. Bismayer, Thermal behavior of dental enamel and geologic apatite: an infrared spectroscopic study, Am. Mineral. 88 (2003) 1866–1871.
[58] S. Elgharbi, K. Horchani-Naifer, M. Ferid, Investigation of the structural and mineralogical changes of tunisian phosphorite during calcinations, J. Therm. Anal. Calorim. 119 (1) (2015) 265–271.
[59] L. Rodriguez-Lorenzo, J. Hart, K. Gross, Influence of fluorine in the synthesis of apatites. Synthesis of solid solutions of hydroxy-fluorapatite, Biomaterials 24 (2003) 3777–3785.
[60] P. Regner, A. Lasaga, R. Berner, Mechanism of CO_3 substitution in carbonate-fluorapatite: evidence from FTIR Spectroscopy, 13C NMR and quantum mechanical calculations, Am. Mineral. 79 (1994) 809–818.
[61] H. Mason, F. McCubbin, A. Smirnov, B. Phillips, Solid-state NMR and IR spectroscopic investigation of the role of structural water and F in carbonate-rich fluorapatite, Am. Mineral. 94 (2009) 507–516.
[62] G.S. Polymeris, G. Kitis, D. Afouxenidis, I.K. Sfampa, N.C. Tsirliganis, A. Rousaki, E. Kouloumpi, K.M. Paraskevopoulos, Mediterranean Archaeology and Archaeometry, 13, 3, pp. 93–103.
[63] V. Pagonis, S. Bernier, F.M. Vieira, S. Steele, The effect of crystal size on tunneling phenomena in luminescent nanodosimetric materials, Nucl. Inst. Methods Phys. Res. B 412 (2017) 198–206 (2017).